Averaged dynamics of soliton molecules in dispersion-managed optical fibers

S. M. Alamoudi,[1] U. Al Khawaja,[2] and B. B. Baizakov[3]
[1]*Department of Physics, King Fahd University of Petroleum and Minerals, Dhahran 31261, Saudi Arabia*
[2]*Physics Department, United Arab Emirates University, P.O. Box 15551, Al-Ain, United Arab Emirates*
[3]*Physical-Technical Institute, Uzbek Academy of Sciences, 100084 Tashkent, Uzbekistan*
(Received 3 November 2013; published 13 May 2014)

The existence regimes and dynamics of soliton molecules in dispersion-managed (DM) optical fibers have been studied. Initially we develop a variational approximation to describe the periodic dynamics of a soliton molecule within each unit cell of the dispersion map. The obtained system of coupled equations for the pulse width and chirp allows to find the parameters of DM soliton molecules for the given dispersion map and pulse energy. Then by means of a scaling transformation and averaging procedure we reduce the original nonlinear Schrödinger equation (NLSE) with piecewise-constant periodic dispersion to its counterpart with constant coefficients and additional parabolic potential. The obtained averaged NLSE with expulsive potential can explain the essential features of solitons and soliton molecules in DM fibers related to their energy loss during propagation. Also, the model of averaged NLSE predicts the instability of the temporal position of the soliton, which may lead to difficulty in holding the pulse in the middle of its time slot. All numerical simulations are performed using the parameters of the existing DM fiber setup and illustrated via pertinent examples.

DOI: 10.1103/PhysRevA.89.053817 PACS number(s): 42.81.Dp, 42.65.Re, 42.79.Sz

I. INTRODUCTION

During the past two decades the amount of information transmitted via optical fiber communication systems has increased enormously. The high performance of modern communication lines is provided by an optical fiber [1], where the information is encoded and transmitted as a sequence of light pulses. Despite the very high data rate achieved today (∼50 TB/s over single fiber), there is urgent demand for even more capacity of the fiber line, originating from the needs of telecommunications and the Internet. Different approaches are being pursued to address the capacity problem, such as improving the transmission properties of the optical fiber, laying additional parallel cables, and using the information coding schemes going beyond the binary format, which is currently employed. Among the above-mentioned approaches, using the extended alphabet, where a bound state of two or more optical solitons called a *soliton molecule* serves as a new carrier of information units [2], seems to be particularly appealing because it employs already existing optical fiber lines, and also the soliton format takes care of the nonlinearity of the fiber, which is the subject of concern in all other competing formats.

It is appropriate to recall that solitons are self-localized wave packets that can propagate along waveguides, preserving their shape and velocity, and exhibit particlelike collisions with each other. Bright solitons emerge from the fine balance between the dispersive broadening and the nonlinear self-focusing of the wave packet. When the optical soliton was theoretically predicted [3] and experimentally observed [4], there was a promising idea that it can be used as an information carrier in optical fiber communication systems [5] due to its exceptional robustness against perturbations. In addition, the nonlinearity of the optical fiber, considered to be a nuisance in linear systems, has been used as an advantage in this case as it provides the soliton's self-healing property. However, some other detrimental effects like four-wave mixing and Gordon-Haus timing jitter [6] have imposed difficulties for progress in this direction. Later the concept of dispersion management (DM) and DM solitons was put forward (for a recent review see Ref. [7]), which allowed to suppress these adverse effects, and eventually led to the realization of several commercial soliton-based optical fiber communication systems. An interesting chronicle of the growth of the telecommunications industry, including fiber optic systems, is given in Ref. [1].

Recent progress in using solitons for information transfer is linked to the observation that solitons in DM fibers can form stable bound states called soliton molecules and to the realization of their potential for enhancing the capacity of the communication system via extension of the coding alphabet [2]. The binding mechanism of solitons in the molecule was proposed in Ref. [8]. The proof-of-principle demonstration of the data transmission via optical fiber using the extended alphabet [logical *zero*, *one* (single soliton), *two* (two-soliton molecule), and *three* (three-soliton molecule)] was recently reported in Refs. [9,10]. The quaternary coding scheme doubles the rate of information transfer compared to the binary case according to the law $\sim\log_2 M$, where M is the number of "letters" in the alphabet. The practical implementation of this novel approach requires extensive research on the existence regimes, stability, mutual interactions, and propagation dynamics of soliton molecules in DM fibers.

Soliton molecules must not be confused with higher-order soliton solutions of the standard nonlinear Schrödinger equation (NLSE) $u(\tau) = N\mathrm{sech}(\tau)$, which also propagate along the fiber by periodically changing their shape without emitting any radiation for integer N. The higher-order soliton is a superposition of several solitons bound together at the same temporal position, e.g., $\tau = 0$, whereas in the molecule solitons are separated by some temporal distance. In contrast to soliton molecules, which normally possess significant binding energy and are therefore quite robust, higher-order solitons can easily disintegrate into constituent solitons, moving away from each other under weak perturbations. Such perturbations may originate from imperfections of the fiber, mutual interaction of pulses, etc. Due to their low tolerance toward perturbations the higher-order solitons are not preferred for optical communications.

The binding mechanism of temporal soliton molecules allows to calculate the potential of interaction as a function of the separation between solitons using the perturbation theory [8,10]. The position of the minimum and the depth of the potential correspond, respectively, to the equilibrium separation and the binding energy of the molecule. To break the molecule into separate stable solitons one has to apply a strong enough perturbation, for instance by setting the solitons into motion in opposite directions with sufficient kinetic energy. Similarly, when two solitons form a stable molecule, the energy released is equal to the molecule's binding energy. We estimate the potential of interaction and binding energy of soliton molecules by means of variational approximation.

A recent interesting discovery was the observation of higher-order equilibrium states of soliton molecules in numerical experiments [11]. In addition to the stable ground state of the molecule, characterized by a minimal separation between opposite-phase solitons, where attractive and repulsive forces acting on solitons are balanced out, a multitude of larger separations are found to exist, where forces acting on solitons again cancel each other. Solitons placed at these temporal separations also stay together as a molecule, while propagating along the fiber. The binding energy of the molecule is found to be lower for higher-order equilibrium states. These equilibrium states come in a sequence, alternatingly stable and unstable [11]. In order to observe higher-order equilibria of soliton molecules one has to prepare the molecule's waveform with sufficiently high precision by means of special numerical techniques. In reality, the continuous emission of linear waves from the soliton during its propagation along the fiber and some inevitable perturbations make the experimental observation of the higher-order equilibria of soliton molecules rather challenging. Thus far, only the stable ground state for the opposite-phase soliton pairs [2,9–11] and the unstable ground state for the in-phase soliton pairs [11] were experimentally observed. We employ the Gauss-Hermite trial functions, which are good for analytic calculations but insufficiently accurate for detecting the higher-order equilibria of soliton molecules. The theory of averaged dynamics of soliton molecules, developed in subsequent sections, allows to reveal a fundamental mechanism of energy emission from propagating solitons. Such energy loss contributes to the destruction of the higher-order equilibria of soliton molecules.

In this work we study the existence regimes and dynamics of soliton molecules in DM fibers by analytical and numerical means. First we develop a variational approach (VA) to find the stationary shape of the molecule and equilibrium separation between solitons in the molecule. At this stage we obtain two coupled ordinary differential equations (ODEs) for the temporal separation between solitons and the chirp parameter, which describes the fast dynamics of the molecule within a unit cell of the DM fiber. Although the derived ODE system is capable of describing the propagation of the molecule for arbitrary distance, long-haul transmission of DM solitons and molecules is convenient to explore using the averaged NLSE. The averaged NLSE can help to specify the existence regimes of solitons and molecules, and to elucidate the physical mechanism by which they lose energy and eventually disintegrate in conservative DM fibers.

The paper is organized as follows. In Sec. II we introduce the NLSE which governs the pulse propagation in DM fibers. Here we also present the parameters of the DM fiber used in our calculations. In Sec. III we develop the VA for the fast dynamics of solitons and molecules and compare its predictions with the results of partial differential equation simulations. Then we derive in Sec. IV the averaged NLSE and determine its coefficients using the VA. Here we also perform the analysis of the pulse propagation in the NLSE with inverted parabolic potential. In Sec. V we summarize our findings.

II. THE GOVERNING EQUATION

The propagation of optical pulses in fibers with inhomogeneous parameters is described by the following nonlinear Schrödinger equation:

$$i\frac{\partial E}{\partial z} - \frac{\beta(z)}{2}\frac{\partial^2 E}{\partial t^2} + \Gamma(z)|E|^2 E = ig(z)E, \tag{1}$$

where $E(z,t)$ [$|E|^2$ (W)], z [m], and t [s] are, respectively, the complex envelope of the electric field, the propagation distance, and the retarded time. The coefficients $\beta(z)$ (s^2/m), $\Gamma(z)$ [1/(W m)], and $g(z)$ [1/m] represent the fiber's group velocity dispersion (GVD), nonlinearity, and gain or loss parameter, respectively. Here and below in square brackets we show the physical unit of the corresponding variable.

For qualitative analysis and numerical simulations it is convenient to reduce Eq. (1) to dimensionless form. At first we eliminate the gain or loss term via a new variable $u(z,t)$ [$|u|^2$ (W)], following Ref. [12]:

$$E(z,t) = a(z)u(z,t), \quad a(z) = a_0 \exp\left[\int_0^z g(\xi)d\xi\right], \tag{2}$$

where a_0 is a dimensionless constant. The new complex function $u(z,t)$ satisfies the equation

$$i\frac{\partial u}{\partial z} - \frac{\beta(z)}{2}\frac{\partial^2 u}{\partial t^2} + \gamma(z)|u|^2 u = 0, \tag{3}$$

where $\gamma(z) = a^2(z)\Gamma(z)$ is the fiber's effective nonlinearity. Now we convert Eq. (3) into standard form with constant nonlinearity by introducing the new coordinate z' [1/W] defined by $z'(z) = \int_0^z \gamma(\xi)d\xi$:

$$i\frac{\partial u}{\partial z'} - \frac{\beta'(z')}{2}\frac{\partial^2 u}{\partial t^2} + |u|^2 u = 0, \tag{4}$$

where $\beta'(z') = \beta(z')/\gamma(z')$ [W s^2] is the fiber's effective dispersion, characterizing both the fiber's GVD and its nonlinearity. The original parameters $\beta(z)$, $\Gamma(z)$, and $g(z)$ in Eq. (1) are periodic functions of propagation distance with common period L, while the effective dispersion $\beta'(z')$ in Eq. (4) is a periodic function with period defined by

$$L' = \int_0^L \gamma(\xi)d\xi = L^+\gamma^+ + L^-\gamma^- \quad [1/\mathrm{W}]. \tag{5}$$

To obtain the final equation we introduce dimensionless variables

$$q(Z,T) = u(z',t)\sqrt{L'}, \quad Z = z'/L', \quad T = t/\tau_m, \tag{6}$$

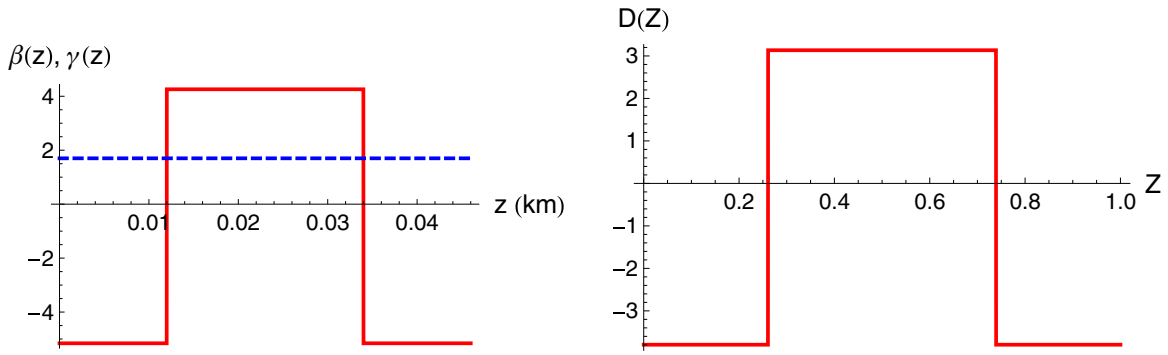

FIG. 1. (Color online) Dispersion profile for one period of the DM map. The solid (red) line represents the piecewise-constant dispersion, and the dashed (blue) line is the parameter of nonlinearity. Left: Profile for the original Eq. (3), where the dispersion $\beta(z)$ and nonlinearity $\gamma(z)$ are given in units of $\mathrm{ps}^2/\mathrm{km}$ and $1/(\mathrm{W\ km})$, respectively. Right: Profile for the reduced Eq. (7), where all quantities are dimensionless. Note that here the coefficient of nonlinearity is equal to 1 and is not shown in Eq. (7) or figure.

where τ_m is the characteristic time scale equal to the pulse duration of the laser source τ_{FWHM}. In terms of these variables the dimensionless governing equation acquires the form

$$i\frac{\partial q}{\partial Z} - \frac{D(Z)}{2}\frac{\partial^2 q}{\partial T^2} + |q|^2 q = 0, \tag{7}$$

where $D(Z) = \beta'(Z)L'/\tau_m^2$ represents the fiber's dimensionless effective dispersion. To show the results in dimensional variables we solve the equation

$$\int_0^z \gamma(\xi)d\xi = ZL' \tag{8}$$

with respect to z [m], for given dimensionless propagation distance Z, the period L' [1/W], and known nonlinear map function $\gamma(z)$ [1/(W m)]. The original time t [s] and field amplitude u [$\sqrt{\mathrm{W}}$] are restored via Eq. (6). Note that $z = L$ corresponds to $Z = 1$, in accordance with Eq. (5).

In the absence of a gain or loss term in Eq. (1), i.e., $g(z) = 0$,

$$a(z) \equiv a_0, \quad a_0 = \left(\frac{L}{\int_0^L \exp\left[2\int_0^z g(\xi)d\xi\right]dz}\right)^{1/2} = 1. \tag{9}$$

The dimensionless pulse energy is

$$E_0 = \int_{-\infty}^{\infty} |q|^2 dT = \frac{L'}{\tau_m}\int_{-\infty}^{\infty} |u|^2 dt = \frac{L'}{\tau_m}\mathcal{E}_0, \tag{10}$$

where $\mathcal{E}_0$ [J] is the original pulse energy.

A. Parameters of the dispersion map

In the following sections we employ the DM map parameters, corresponding to the setup of Refs. [9,10], for laser wavelength $\lambda = 1540$ nm:

$\beta_2^+ = +4.259\,[\mathrm{ps}^2/\mathrm{km}]$, $\gamma^+ = 1.7\,[1/(\mathrm{W/km})]$, and

$L^+ = 22\,[\mathrm{m}]$ (positive GVD fiber),

and

$\beta_2^- = -5.159\,[\mathrm{ps}^2/\mathrm{km}]$, $\gamma^- = 1.7\,[1/(\mathrm{W/km})]$, and

$L^- = 24\,[\mathrm{m}]$ (negative GVD fiber).

The period of the original DM map is $L = L^+ + L^- = 46$ [m]. For the effective dispersion in Eq. (4) the period is $L' = \gamma^+ L^+ + \gamma^- L^- = 0.078$ [1/W]. The path averaged dispersion and nonlinearity are equal to

$$\bar{\beta}_2 = (\beta_2^+ L^+ + \beta_2^- L^-)/L = -0.655 \quad [\mathrm{ps}^2/\mathrm{km}],$$
$$\bar{\gamma} = (\gamma^+ L^+ + \gamma^- L^-)/L = 1.7 \quad [1/(\mathrm{W\,km})].$$

The characteristic time, length, and energy scales are given below:

$$\begin{aligned}
\tau_{\mathrm{FWHM}} &= 0.25\,[\mathrm{ps}],\\
T_0 &= \tau_{\mathrm{FWHM}}/1.67 = 0.15\,[\mathrm{ps}]\ (\text{pulse duration}),\\
L_D &= T_0^2/|\bar{\beta}_2| = 0.034\,[\mathrm{km}]\\
&\quad (\text{dispersion length}), \quad \text{and}\\
S &= (|\beta_2^+ - \bar{\beta}_2|L^+ + |\beta_2^- - \bar{\beta}_2|L^-)/\tau_{\mathrm{FWHM}}^2\\
&= 3.459\ (\text{strength of the map}).
\end{aligned}$$

From the above-presented data we get the dimensionless map parameters:

$$\begin{aligned}
D_1 &= (\beta_2^-/\gamma^-)\left(L'/\tau_{\mathrm{FWHM}}^2\right) = -3.796,\\
L_1 &= L^-\gamma^-/L' = 0.522,\\
D_2 &= (\beta_2^+/\gamma^+)\left(L'/\tau_{\mathrm{FWHM}}^2\right) = +3.135,\\
L_2 &= L^+\gamma^+/L' = 0.478,\\
\Delta D &= (D_1 L_1 + D_2 L_2)/(L_1 + L_2) = -0.482,\\
L_1 + L_2 &= 1.
\end{aligned}$$

Figure 1 shows the dispersion profiles for the original and reduced governing equations.

III. THE VARIATIONAL APPROACH FOR FAST DYNAMICS OF SOLITON MOLECULES

Propagation of a DM soliton is characterized by fast variation of the pulse shape within each period of the DM map and slow variations on longer distances when observed stroboscopically, i.e., once per dispersion period. The periodic dynamics is compromised by different imperfections of the fiber, continuous emission of linear waves by the soliton, and

the nonperfect initial shape of the DM soliton injected into the fiber. To compensate for the power loss and other distortions, in practice the pulses are regenerated by amplifiers which are equidistantly installed along the fiber line.

The variational approach, initially developed to describe optical soliton propagation in homogeneous fibers [13], later was successfully applied to DM solitons [14] and antisymmetric solitons in DM fibers [15,16]. The advantages and disadvantages of the VA as compared to other methods of exploring DM solitons are discussed in Refs. [17,18]. Below we elaborate the VA for two- and three-soliton molecules in DM fibers, based on the reduced NLSE (7).

Equation (7) can be obtained from the following Lagrangian density (for tidier notations we again use small letters instead of capitals):

$$\mathcal{L} = \frac{i}{2}(qq_z^* - q^*q_z) - \frac{d(z)}{2}|q_t|^2 - \frac{1}{2}|q|^4. \tag{11}$$

To derive the VA equations we consider the shape of the soliton molecule in general form [14,19],

$$q(z,t) = \frac{1}{\tau^{1/2}} f(t/\tau) e^{i\alpha t^2 + i\sigma}, \tag{12}$$

where $\alpha(z)$ and $\sigma(z)$ are the chirp parameter and phase, $\tau(z)$ is the pulse duration (proportional to the separation between solitons in the molecule), and $f(x)$ is the real function which represents the stationary shape of the soliton molecule. The energy of the pulse is [subscript zero in Eq. (10) is dropped]

$$E = \int_{-\infty}^{\infty} |q|^2 dt = \int_{-\infty}^{\infty} f^2(x) dx, \quad x = t/\tau. \tag{13}$$

Substitution of the trial function (12) into Eq. (11) yields the Lagrangian density

$$\mathcal{L} = \tau\alpha_z x^2 f^2 + \frac{\sigma_z}{\tau} f^2 - \frac{1}{2}\frac{d(z)}{\tau^3} f_x^2 - 2\,d(z)\tau\alpha^2 x^2 f^2 - \frac{1}{2\tau^2} f^4. \tag{14}$$

The averaged Lagrangian is obtained by integrating the last expression over the reduced time variable,

$$L = \alpha_z \tau^2 \int_{-\infty}^{\infty} x^2 f^2 dx + \sigma_z \int_{-\infty}^{\infty} f^2 dx - \frac{d(z)}{2\tau^2} \int_{-\infty}^{\infty} f_x^2 dx - 2d(z)\alpha^2\tau^2 \int_{-\infty}^{\infty} x^2 f^2 dx - \frac{1}{2\tau} \int_{-\infty}^{\infty} f^4 dx, \tag{15}$$

with a few integral constants, determined solely by the pulse shape $f(x)$. The Euler-Lagrange equations with respect to variational parameters τ, α, and σ give rise to a coupled set of ODEs:

$$\tau_z = -2\,d(z)\alpha\tau, \tag{16}$$

$$\alpha_z = -2\,d(z)\left(\frac{c_1}{4\tau^4} - \alpha^2\right) - \frac{c_2}{4\,\tau^3}, \tag{17}$$

where

$$c_1 = \int_{-\infty}^{\infty} f_x^2 dx \Big/ \int_{-\infty}^{\infty} x^2 f^2 dx, \qquad c_2 = \int_{-\infty}^{\infty} f^4 dx \Big/ \int_{-\infty}^{\infty} x^2 f^2 dx. \tag{18}$$

We adopt the following trial functions $f(x)$ to specify the shapes of the pulses and define the corresponding parameters:

$$\text{single soliton,} \quad f(x) = A\,e^{-x^2}, \quad E = A^2\sqrt{\frac{\pi}{2}}, \quad c_1 = 4, \quad c_2 = \frac{4E}{\sqrt{\pi}}; \tag{19}$$

$$\text{two-soliton molecule,} \quad f(x) = A\,x\,e^{-x^2}, \quad E = \frac{A^2}{4}\sqrt{\frac{\pi}{2}}, \quad c_1 = 4, \quad c_2 = \frac{E}{\sqrt{\pi}}; \tag{20}$$

$$\text{three-soliton molecule,} \quad f(x) = A\,(4x^2 - 1)\,e^{-x^2}, \quad E = A^2\sqrt{2\pi}, \quad c_1 = 4, \quad c_2 = \frac{41\,E}{80\,\sqrt{\pi}}. \tag{21}$$

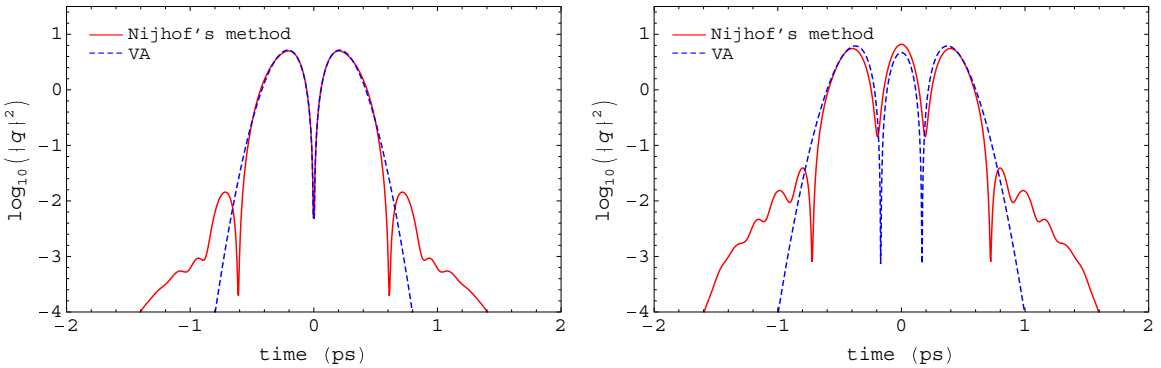

FIG. 2. (Color online) Pulse shapes of the two-soliton molecule (left) and three-soliton molecule (right) in logarithmic scale. Solid (red) lines correspond to waveforms found by Nijhof's method [20] applied to the original NLSE (7), while dashed (blue) lines are the prediction of VA Eqs. (16) and (17). Appreciable deviations of the two waveforms are seen only in far tails, where the pulse amplitude is less than a percent of the maximum value. The parameters for the two-soliton molecule are $E_0 = 10.448$ (in original units $\mathcal{E}_0 = 20$ pJ), $\tau_0 = 1.1828$, and $A_0 = \frac{2}{\tau_0}\sqrt{\frac{E_0}{\tau_0}\sqrt{2/\pi}} = 4.489$. For the three-soliton molecule, $E_0 = 15.672$ ($\mathcal{E}_0 = 30$ pJ), $\tau_0 = 1.333$, and $A_0 = \sqrt{\frac{E_0}{\tau_0\sqrt{2\pi}}} = 2.166$. The pulse power $|q|^2$ is shown in dimensionless units according to Eq. (6).

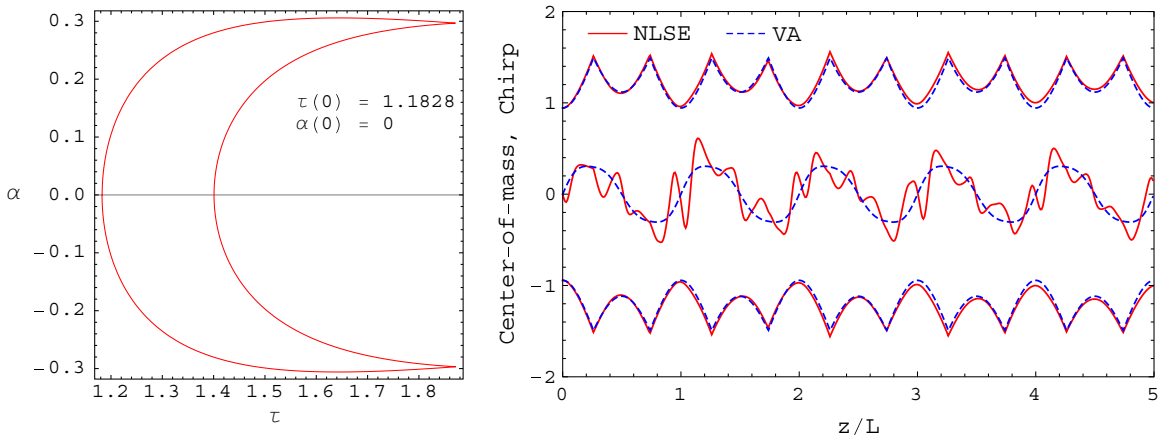

FIG. 3. (Color online) Left: Closed phase trajectory indicates that the fixed point $\tau(0) = 1.1828$, $\alpha(0) = 0$ corresponds to the periodic solution of the system (16) and (17) for a two-soliton molecule with energy $E = 10.448$, shown in Fig. 2. Right: The solution of the NLSE (7) with the initial pulse shape predicted by the VA shows that solitons in the two-soliton molecule perform oscillatory motion periodically reducing and increasing the temporal separation between their center-of-mass positions (top and bottom curves). The evolution of the chirp parameter (middle curve) shows qualitative agreement with the VA.

The fixed point (τ_0,α_0) of the coupled system (16) and (17), which can be found using the Nijhof method for VA models [20], defines the stationary shapes of the pulses with given energy E and DM map function $d(z)$. In Fig. 2 we illustrate the shapes of the two-soliton and three-soliton molecules, which are found by solving the VA system (16) and (17) and compare with the corresponding results of the Nijhof method applied to the original Eq. (7). In Fig. 3 we show the phase trajectory for the periodic solution of the VA system (16) and (17) and temporal center-of-mass positions of solitons in the two-soliton molecule while it propagates along the fiber. The center-of-mass position of the right/left soliton is calculated from the solution of the VA system (16) and (17) as $\tau_{\text{c.m.}}(z) = \pm\tau(z)\sqrt{2/\pi}$, while for the NLSE (7) the corresponding formula is

$$\tau_{\text{c.m.}}(z) = \pm\frac{2}{E_0}\int_0^\infty t\,|q(z,t)|^2 dt, \tag{22}$$

where in actual calculations we use the temporal domain's half length as the upper limit of the integration. For evaluation of the pulse width and chirp parameter from the solution of Eq. (7) we employ the following expressions [20]:

$$\begin{aligned}\tau(z) &= \left(\frac{4}{3E}\int_{-\infty}^{\infty} t^2|q(z,t)|^2 dt\right)^{1/2},\\ \alpha(z) &= \frac{\int_{-\infty}^{\infty}\text{Im}[q^2(z,t)q_t^*(z,t)]dt}{\int_{-\infty}^{\infty}|q(z,t)|^4 dt}.\end{aligned} \tag{23}$$

As can be seen from Fig. 3 the dynamics of the pulse width is described by the VA equations quite accurately, while for the chirp parameter the agreement is only qualitative. It should be noted that although the chirp parameter shows complicated behavior within the map period, the "zero chirp" condition in the middle of each anomalous GVD fiber is well satisfied.

IV. AVERAGED EQUATION FOR SOLITON MOLECULES IN DM FIBERS

Long-haul propagation of soliton molecules in DM fibers is convenient to study using the averaged NLSE. The averaging procedure was developed in Refs. [14,19]. Below we use the approach based on the scaling arguments proposed in Ref. [21] and look for the solution of Eq. (7) in the form (capital letters changed to lower case)

$$q(z,t) = w(z,t)\,e^{i\,\alpha(z)\,t^2}, \tag{24}$$

where $\alpha(z)$ is the chirp parameter. Inserting this into the governing Eq. (7) we obtain

$$\begin{aligned}&i(w_z - 2d\alpha t\,w_t) - \frac{d}{2}w_{tt} + (2d\alpha^2 - \alpha_z)\,t^2 w + |w|^2 w\\ &\quad = id\alpha w.\end{aligned} \tag{25}$$

By introducing the new time (x) and amplitude (b) functions

$$x = t/\tau(z), \quad w(z,t) = b(z)\,v(z,x), \tag{26}$$

the last equation can be reduced to the form

$$\begin{aligned}&i\left(bv_z + b_z v - \frac{bt\tau_z}{\tau^2}v_x - \frac{2bd\alpha t}{\tau}v_x\right) - \frac{bd}{2\tau^2}\,v_{xx}\\ &\quad -(\alpha_z - 2d\alpha^2)t^2 bv + b^3|v|^2 v = id\alpha bv.\end{aligned} \tag{27}$$

When the following relations are satisfied,

$$b_z = d\,\alpha\,b, \quad \tau_z = -2\,d\,\alpha\,\tau, \tag{28}$$

the NLSE with a parabolic potential results from Eq. (27):

$$iv_z - \frac{d}{2\tau^2}\,v_{xx} + b^2|v|^2 v - (\alpha_z - 2d\alpha^2)\tau^2 x^2 v = 0. \tag{29}$$

The amplitude function is linked to the pulse width as $b(z) = \beta/\sqrt{\tau(z)}$, which can be readily verified from Eq. (28). The constant β is specified by the selected trial function. Now applying the averaging procedure to Eq. (29) we obtain in leading order

$$i\psi_z + d_0\psi_{xx} + b_0|\psi|^2\psi + k_0 x^2\psi = 0, \tag{30}$$

where $\psi(z,x)$ is the slowly varying core of the DM soliton. The quantities averaged over one dispersion period are defined as $d_0 = -\frac{1}{2}\langle d(z)/\tau^2(z)\rangle$, $b_0 = \beta^2\langle 1/\tau(z)\rangle$, and $k_0 = \langle[2d(z)\,\alpha^2(z) - \alpha_z(z)]\,\tau^2(z)\rangle$. The averaging is performed as $\langle\phi(z)\rangle = \int_0^1 \phi(z)\tau(z)dz/\int_0^1 \tau(z)dz$ (for the reduced map period $L = 1$). In numerical implementation of the averaging procedure we employ the periodic solution of VA Eqs. (16) and (17). In particular from Eq. (17) it follows that $k_0 = (c_1/2)\langle d(z)/\tau^2(z)\rangle + (c_2/4)\langle 1/\tau(z)\rangle$, with constants c_1,c_2 given by Eq. (18). For the DM map parameters specified in Sec. II all coefficients of Eq. (30) appear to be positive ($d_0 > 0$, $b_0 > 0$, $k_0 > 0$); therefore, we have gotten the NLSE with anomalous dispersion, focusing nonlinearity, and inverted parabolic potential. This equation is formally similar to the quantum-mechanical equation for a wave packet, evolving under the effective potential

$$U(z,x) = -b_0\,|\psi(z,x)|^2 - k_0\,x^2. \tag{31}$$

The stationary solution $\psi(z,x) = \varphi(x)e^{i\lambda z}$ can be found from the initial value problem with respect to variable x,

$$d_0\,\varphi_{xx} + b_0\,\varphi^3 + k_0\,x^2\,\varphi - \lambda\,\varphi = 0, \tag{32}$$

and suitable initial conditions $\varphi(0)$ and $\varphi_x(0)$.

It is appropriate to mention that Eq. (30) with an additional gain or loss term was previously considered also in other contexts, such as the nonlinear compression of chirped optical solitary waves [22], and with regard to integrability issues [23–26].

A. The variational approach for averaged NLSE

To study the evolution of pulses governed by Eq. (30) we develop the VA. The corresponding Lagrangian density is

$$\mathcal{L} = \frac{i}{2}(\psi\psi_z^* - \psi^*\psi_z) + d_0|\psi_x|^2 - k_0x^2|\psi|^2 - \frac{b_0}{2}|\psi|^4. \tag{33}$$

The trial function is of the form

$$\psi(x,t) = A\,\eta(x)\,e^{-(x-\xi)^2/\tau^2 + i\alpha(x-\xi)^2 + iv(x-\xi) + i\varphi}, \tag{34}$$

where $A(z)$, $\tau(z)$, $\xi(z)$, $v(z)$, $\alpha(z)$, and $\varphi(z)$ are variational parameters, designating the pulse amplitude, width, center-of-mass position, velocity, chirp, and phase, respectively. The auxiliary function $\eta(x)$ is introduced for convenience and defines the type of the pulse. Specifically for a single soliton $\eta(x) = 1$, for a two-soliton molecule $\eta(x) = x$, and for a three-soliton molecule $\eta(x) = 4x^2 - 1$.

It is instructive to start by considering the existence and dynamics of a single soliton on top of an inverted parabolic potential. The integration $L = \int_{-\infty}^{\infty}\mathcal{L}\,dx$ using the trial function (34) with $\eta(x) = 1$ gives rise to the following effective Lagrangian:

$$\frac{L}{E} = \frac{1}{4}\tau^2\alpha_z - \xi_z^2 + \varphi_z + \frac{d_0}{\tau^2} + d_0\tau^2\alpha^2 + d_0\xi_z^2 - \frac{k_0}{4}\tau^2 - k_0\xi^2 - \frac{b_0E}{2\sqrt{\pi}\tau}, \tag{35}$$

where the pulse energy $E = A^2\tau\sqrt{\pi/2}$ is conserved. Now applying the Euler-Lagrange equations with respect to the variational parameters, we get the ODE system for the pulse width and its center-of-mass position,

$$\tau_{zz} = \frac{16d_0^2}{\tau^3} + 4d_0k_0\tau - \frac{4d_0b_0E}{\sqrt{\pi}\,\tau^2}, \tag{36}$$

$$\xi_{zz} = -k_0/(d_0 - 1)\xi. \tag{37}$$

The system for the two-soliton and three-soliton molecules will be similar, with only the rescaled energy coefficient, $E \to E/4$ for the former case and $E \to (41/320)E$ for the latter case [see the coefficient c_2 in Eqs. (20) and (21)]. As can be seen from this system, the center of mass and internal dynamics of the soliton are decoupled. This is due to the property of a parabolic potential and is the manifestation of the Ehrenfest theorem. (Its validity for the nonlinear Schrödinger equation with linear and parabolic potentials was proved in Ref. [27].) In other types of potentials these two degrees of freedom are coupled. In fact the equation for the center of mass is the harmonic oscillator equation with a purely imaginary frequency $\omega^2 = k_0/(d_0 - 1) < 0$, since in practical situations $k_0 > 0$ and $d_0 < 1$. Therefore, the center of mass of the soliton is unstable against sliding down an inverted parabola with exponentially increasing distance from the origin

$$\xi(z) = \xi(0)\,e^{Kz}, \quad \text{where} \quad K = \sqrt{k_0/|d_0 - 1|} > 0. \tag{38}$$

The equation for the pulse width, Eq. (36), is similar to the equation of motion for a unit mass particle in the anharmonic potential

$$\tau_{zz} = -\frac{dU}{d\tau}, \quad U(\tau) = \frac{8d_0^2}{\tau^2} - 2d_0k_0\tau^2 - \frac{4d_0b_0E}{\sqrt{\pi}\,\tau}, \tag{39}$$

which is depicted in Fig. 4. The minimum of this potential is found from the solution of the quartic equation

$$\tau^4 - m\tau + n = 0, \quad m = \frac{b_0E}{\sqrt{\pi}\,k_0}, \quad n = \frac{4d_0}{k_0}, \tag{40}$$

and corresponds to the stationary width of the soliton. For a given pulse energy E this defines the shape of the soliton according to the ansatz (34). At some critical energy $E_{\rm cr}$ the local minimum in this potential disappears, which means that Eq. (30) does not support solitons and molecules with energy below $E_{\rm cr}$. The value of the critical energy can be found from the condition that Eq. (40) has a real solution, which takes place if $m > 4(n/3)^{3/4}$ or, in terms of energy,

$$E > E_{\rm cr} = \frac{2^{7/2}\,\pi^{1/2}}{3^{3/4}}\frac{d_0^{3/4}\,k_0^{1/4}}{b_0} \simeq 8.8\,\frac{d_0^{3/4}\,k_0^{1/4}}{b_0}. \tag{41}$$

In fact the shape of the potential $U(\tau)$ gives the evidence that solitons and molecules in the system are metastable. In the same figure (Fig. 4) we compare the pulse profiles obtained by solution of the stationary state Eq. (32) with the prediction of VA. The parameter λ for Eq. (32) is obtained using the shooting method, where the pulse energy $E = \int|\varphi(x)|^2dx$ is minimized and initial conditions $\varphi(0) = A$, $\varphi_x(0) = 0$ are used. As can be seen from this figure, the deviation between the two wave profiles is notable at far tails of the pulse, where the field intensity significantly decreases. The wavy tails on the numerically exact pulse profile, found from the solution of Eq. (32), indicate the existence of waves reflected from (and partially transmitted through) the borders of the effective

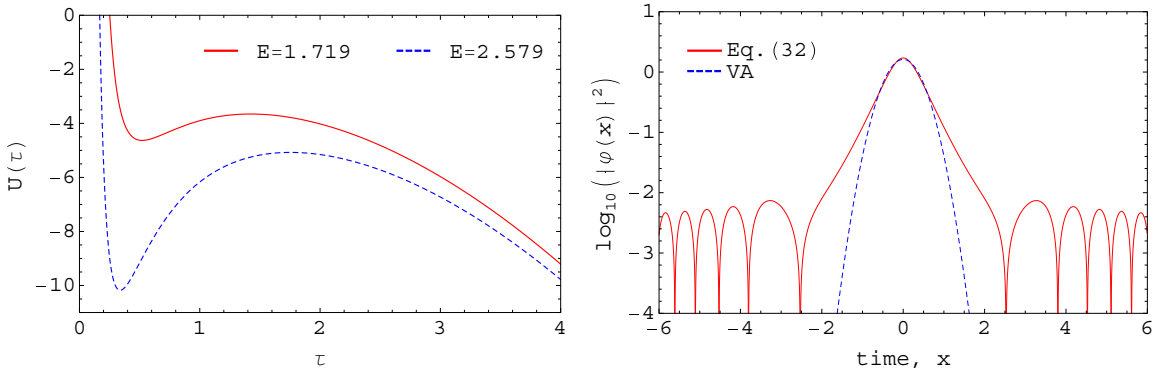

FIG. 4. (Color online) Left: The potential (39) in the effective particle model of VA for two values of the pulse energy. The pulse with greater energy forms a deeper potential well. The stationary amplitude and width of the soliton for $E = 1.7193$, according to VA, are $A = 1.6227$ and $\tau = 0.521$, respectively. The existence of a local maximum and decay at large τ is the evidence of metastability of the stationary state. Right: Comparison between the pulse shapes (in logarithmic scale) obtained by solving the stationary state problem (32) for $\lambda = 4.6132$ and prediction of VA for the same pulse energy. The wavy tails are due to the interference of waves reflecting from the borders of the effective potential (31). Parameters $d_0 = 0.3782$, $b_0 = 3.0917$, and $k_0 = 0.6734$ are obtained using the VA Eqs. (16) and (17) for a single DM soliton with energy $E_0 = 5.224$ (in original units $\mathcal{E}_0 = 10$ pJ) and fiber data of Sec. II.

potential (31). The waves escaping the effective potential contribute to the continuous outflow of energy from the soliton propagating along the fiber, and that is the fundamental source of its instability in conservative DM fibers.

The "pulse in the effective potential" picture, shown in Fig. 5, is helpful for the analysis of instability issues. The first aspect to be noted is that the height and width of the effective potential barrier in both directions from the pulse are finite and depend on the intensity of the pulse itself. Therefore, a continuous and nonlinearly progressing energy outflow from the soliton takes place via the tunneling effect, whose rate can be estimated by means of the semiclassical WKB method as was done for the matter-wave analog of this problem in Ref. [28]. These authors also have shown that the rate of energy outflow (number of particles for condensates) nonlinearly increases, eventually leading to disintegration of the soliton. The second aspect is the instability of the center-of-mass position of the soliton against sliding down an inverted parabola. According to Eq. (38) any small departure of the center-of-mass position from the origin (the top of the inverted parabola) in either direction will exponentially grow.

To verify the above conclusions following from our model, we performed numerical simulations of the pulse propagation governed by Eq. (30). When we introduce the wave profile predicted by VA, which slightly differs from the solution of Eq. (32), as an initial condition to Eq. (30), the pulse quickly adjusts itself by performing damped oscillations of its amplitude, and then continuously decays both in energy and amplitude, as shown in Fig. 6. The frequency of oscillations of the amplitude well agrees with the prediction of VA, when we expand the potential (39) near its minimum τ_0 and estimate the corresponding frequency and period $\omega_0 = \sqrt{d^2U/d\tau^2|_{\tau=\tau_0}} \simeq 5.12$, $T_0 = 2\pi/\omega_0 = 1.22$. However, the VA does not take into account the dissipative effects. In numerical simulations we use the absorbing boundary technique [29] to prevent the interference of the soliton with the linear waves, which are otherwise reflected from the integration domain boundaries. To calculate the energy outflow from the soliton, we monitor the amount of energy in the central part of the domain ($x \in [-2,2]$ in Fig. 6) where the bulk of the pulse is confined. The energy loss rate dE/dz is characteristic for the fiber parameters and initial pulse power, which define the coefficients of the averaged NLSE (30). The instability of the center-of-mass

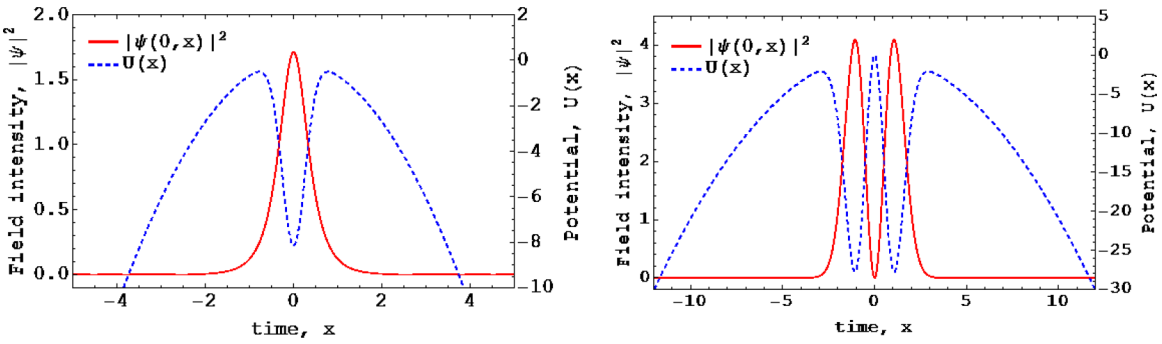

FIG. 5. (Color online) Single soliton (left) and two-soliton molecule (right) of the averaged NLSE (30) are shown by solid (red) lines. The corresponding effective potentials according to Eq. (31) are shown by dashed (blue) lines. The parameters for the single soliton are the same as in Fig. 4, while for the two-soliton molecule the parameters are $d_0 = 0.1978$, $b_0 = 6.7274$, $k_0 = 0.209$, and $E_0 = 10.448$ (in original units $\mathcal{E}_0 = 20$ pJ).

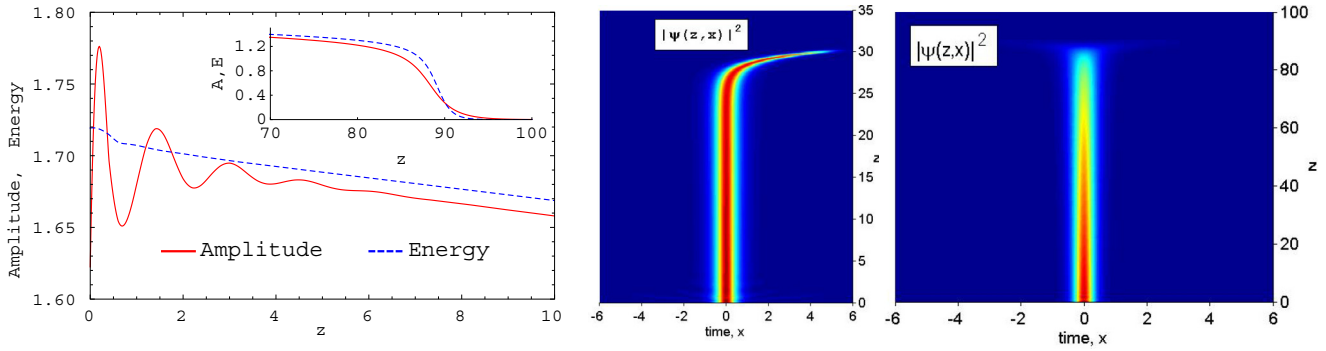

FIG. 6. (Color online) Left: The amplitude and energy of the soliton decay as it propagates along the fiber due to the wave tunneling effect. The inset shows the nonlinear character of the energy loss at longer distances and abrupt disintegration of the pulse at some critical energy. The data are obtained by numerical simulation of Eq. (30) with absorbing boundary conditions. The initial wave is a Gaussian pulse with amplitude $A = 1.6227$ and width $\tau = 0.521$, as predicted by VA. Middle: The soliton slightly displaced from the top of the inverted parabola (by an amount $\Delta x \sim \pm 10^{-3}$) slides down with increasing velocity in the corresponding direction. This instability develops even due to a numerical noise, when the soliton is placed exactly at the origin, $x = 0$. Right: When the calculation is performed with centering of the pulse, a complete disintegration can be observed at sufficiently long propagation distance.

position of the soliton is demonstrated in the middle panel of Fig. 6. If the calculation is performed with centering of the soliton, when at each step its center of mass is held at the origin, we observe complete disintegration of the pulse due to the energy loss, as shown in the right panel of Fig. 6. It should be pointed out that the pulse disintegrates after propagation of a rather long distance of ∼80 DM map periods. For the parameters of the setup [9,10], which is a scale model of a typical fiber line with 40 Gbit/s bit rate using $\tau_{\mathrm{FWHM}} = 7.5$ ps pulses, 80 dispersion periods corresponds to a distance of 3200 km. The critical energy at which the pulse disintegrates, according to the inset of the left panel, is $E_{\mathrm{cr}} \simeq 1.2$. This numerical finding is in good agreement with the prediction of VA Eq. (41), $E_{\mathrm{cr}} = 1.24$.

In fact the above-mentioned mechanism of energy loss sets the limit to attainable robustness of DM solitons and molecules in the given setup. The instability of the center of mass of the soliton will make it difficult to hold the pulse in the middle of its time slot. In Fig. 7 we demonstrate the propagation of two solitons governed by Eq. (30). When two in-phase solitons are initially placed at a separation exceeding some critical value, they move apart with increasing velocity under the effect of the expulsive parabolic potential. If the solitons are placed at a smaller temporal distance, they collide a few times and merge together, and later the combined pulse develops an instability, analogous to the single-soliton case, and slides down the inverted parabola. Similar behavior of two-soliton states was reported in the dissipative counterpart of Eq. (30) in Ref. [26]. An additional fact relevant to coupled soliton propagation in this system is that the out-of-phase solitons always repel each other and diverge from the origin in an accelerated manner.

The main result of our study of pulse propagation governed by the averaged NLSE (30) is that it does not support truly stable solitons and molecules as the original DM Eq. (7) does. Rather it shows that solitons and molecules in the conservative DM fiber are metastable, in terms of both energy and temporal position. For the fiber parameters that we have used, the energy loss amounts to ∼5 % of the initial value at pulse propagation over 10 dispersion periods, which in a typical fiber system using 7.5-ps pulses corresponds to a distance of 400 km. In addition, the model of averaged NLSE allows to find the

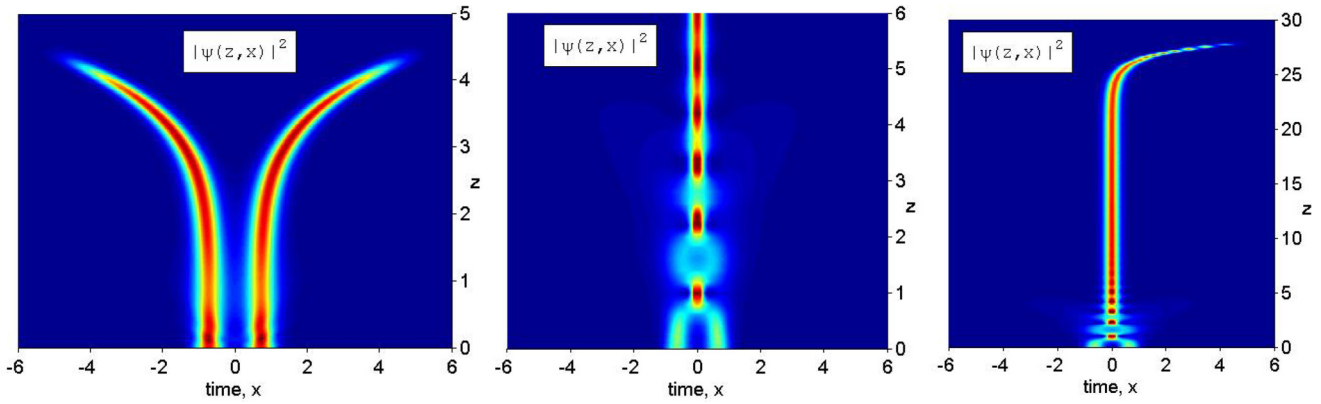

FIG. 7. (Color online) Left: Two in-phase solitons placed sufficiently far from each other ($\Delta x = 0.72$) move apart. Middle: When solitons are placed at a distance ($\Delta x = 0.65$) which is less than some critical value, they collide a few times and merge. Right: Long-distance behavior of the coalescent pulse (of the middle panel) is similar to the single-soliton case, as its center of mass develops instability and slides down the inverted parabola.

existence regimes and identify the limits of stability of solitons and molecules in DM fibers. The inclusion of dissipation and gain into the model may change the results to some degree. This will be a subject for separate study.

V. CONCLUSIONS

We have developed a variational approximation which successfully describes the propagation of soliton molecules in DM fibers. The pulse shapes for a two-soliton molecule and three-soliton molecule, predicted by VA, are shown to be sufficiently close to the numerically exact shapes found by solution of the original DM NLSE. Then we studied the dynamics of solitons and molecules in the averaged NLSE corresponding to the selected DM fiber system. The approach of the averaged NLSE allows to identify the regimes of the existence of solitons and molecules in the original DM system and to reveal the fundamental source of the instability of soliton propagation in DM fibers, which is linked to continuous outflow of energy from the pulse due to the wave tunneling phenomenon. Although the corresponding energy loss rate is rather small, initially amounting to $\sim$0.5% of the input energy per DM map period, it increases nonlinearly and gives rise to disintegration of the pulse at long distances. The model also predicts the instability of the temporal position of the pulse within its time slot. All calculations are performed using the parameters of the existing DM fiber setup [9,10]. The model may provide guidance in further studies of the properties of soliton molecules in DM fibers.

ACKNOWLEDGMENTS

We thank F. Mitschke, A. Hause, and E. N. Tsoy for valuable discussions. U.A.K. and B.B.B. are grateful to the Department of Physics of the KFUPM for the hospitality during their stay. This work is supported by Research Grant No. UAEU-NRF 2011 and KFUPM Research Projects No. RG1214-1 and No. RG1214-2.

[1] Fedor Mitschke, *Fiber Optics: Physics and Technology* (Springer-Verlag, Berlin, 2009).
[2] M. Stratmann, T. Pagel, and F. Mitschke, Phys. Rev. Lett. **95**, 143902 (2005).
[3] A. Hasegawa and F. Tappert, Appl. Phys. Lett. **23**, 142 (1973).
[4] L. F. Mollenauer, R. H. Stolen, and J. P. Gordon, Phys. Rev. Lett. **45**, 1095 (1980).
[5] A. Hasegawa and Y. Kodama, *Solitons in Optical Communications* (Clarendon, Oxford, 1995).
[6] L. F. Mollenauer and J. P. Gordon, *Solitons in Optical Fibers: Fundamentals and Applications* (Academic, San Diego, 2006).
[7] S. K. Turitsyn, G. B. Brandon Bale, and M. P. Fedoruk, Phys. Rep. **521**, 135 (2012).
[8] A. Hause, H. Hartwig, M. Böhm, and F. Mitschke, Phys. Rev. A **78**, 063817 (2008).
[9] P. Rohrmann, A. Hause, and F. Mitschke, Sci. Rep. **2**, 866 (2012).
[10] P. Rohrmann, A. Hause, and F. Mitschke, Phys. Rev. A **87**, 043834 (2013).
[11] A. Hause and F. Mitschke, Phys. Rev. A **88**, 063843 (2013).
[12] A. Maruta, T. Inoue, Y. Nonaka, and Y. Yoshika, IEEE J. Sel. Top. Quantum Electron. **8**, 640 (2002).
[13] D. Anderson, Phys. Rev. A **27**, 3135 (1983).
[14] S. K. Turitsyn, I. Gabitov, E. W. Laedke, V. K. Mezentsev, S. L. Musher, E. G. Shapiro, T. Schafer, and K. H. Spatschek, Opt. Commun. **151**, 117 (1998).
[15] C. Pare and P.-A. Belanger, Opt. Commun. **168**, 103 (1999).
[16] B.-F. Feng and B. A. Malomed, Opt. Commun. **229**, 173 (2004).
[17] V. Cautaerts, A. Maruta, and Y. Kodama, Chaos **10**, 515 (2000).
[18] B. A. Malomed, *Soliton Management in Periodic Systems* (Springer, New York, 2006).
[19] S. K. Turitsyn, JETP Lett. **65**, 845 (1997); S. K. Turitsyn, T. Schäfer, K. H. Spatschek, and V. K. Mezentsev, Opt. Commun. **163**, 122 (1999).
[20] J. H. B. Nijhof, W. Forysiak, and N. J. Doran, IEEE J. Sel. Top. Quantum Electron. **6**, 330 (2000).
[21] Y. Kodama, S. Kumar, and A. Maruta, Opt. Lett. **22**, 1689 (1997).
[22] J. D. Moores, Opt. Lett. **21**, 555 (1996).
[23] K. Nakkeeran, J. Phys. A: Math. Gen. **34**, 5111 (2001).
[24] C. C. Mak, K. W. Chow, and K. Nakkeeran, J. Phys. Soc. Jpn. **74**, 1449 (2005).
[25] Zhiyong Xu, Lu Li, Zhonghao Li, Guosheng Zhou, and K. Nakkeeran, Phys. Rev. E **68**, 046605 (2003).
[26] R. Grimshaw, K. Nakkeeran, C. K. Poon, and K. W. Chow, Phys. Scr. **75**, 620 (2007).
[27] R. W. Hasse, Phys. Rev. A **25**, 583 (1982).
[28] L. D. Carr and Y. Castin, Phys. Rev. A **66**, 063602 (2002).
[29] P. Berg, F. If, P. L. Christiansen, and O. Skovgaard, Phys. Rev. A **35**, 4167 (1987).